HHS Public Access

Author manuscript

Curr Opin Neurobiol. Author manuscript; available in PMC 2021 August 01.

Published in final edited form as:

Curr Opin Neurobiol. 2020 August ; 63: 111–121. doi:10.1016/j.conb.2020.02.011.

Fluorescent Biosensors for Neuronal Metabolism and the Challenges of Quantitation

Dorothy Koveal, **Carlos Manlio Díaz-García**, **Gary Yellen**

Department of Neurobiology, Harvard Medical School, Boston, MA, USA

Abstract

Over the past decade, genetically encoded fluorescent biosensors that report metabolic changes have become valuable tools for understanding brain metabolism. These sensors have been targeted to specific brain regions and cell types in different organisms to track multiple metabolic processes at single cell (and subcellular) resolution. Here, we review genetically encoded biosensors used to study metabolism in the brain. We particularly focus on the principles needed to use these sensors quantitatively while avoiding false inferences from variations in sensor fluorescence that arise from differences in expression level or environmental influences such as pH or temperature.

Introduction

The last ten years have witnessed a revolution in our ability to monitor brain signaling and metabolism using engineered fluorescent biosensors. Although calcium sensors have been used for decades, first in the form of engineered dyes and later genetically encoded biosensors, many more biosensors have recently become available both for signaling (through second messengers, kinases, and reactive oxygen species) and for key metabolites (glucose, ATP, NADH, NADPH, and other metabolic cofactors and intermediates; Figure 1). This review will focus on the general principles needed for informed “responsible use” of metabolic biosensors, which present specific challenges of quantitation and interpretation.

Monitoring neuronal activity at the single-neuron level is the most prominent and wide-spread application of biosensors in neurobiology. Calcium or voltage sensors can reveal action potential activity in large populations of neurons [1–3], and detailed quantitation involves relatively straightforward scoring of the temporal pattern of biosensor fluorescence.

By contrast, monitoring slower metabolic processes in neurons or glial cells requires a different type of quantitation to assess both the baseline levels and magnitude of change in the biosensor target. The quantitative challenges go beyond the difficulties of achieving absolute calibration of the biosensor response; they extend to the difficulty of comparing the relative levels of metabolites in two different cells within the same preparation, and to the more pernicious problem of “aliasing”: when a biosensor appears to report a change in its target analyte even when there has been no change. Critical environmental sensitivities of many biosensors, particularly sensitivity to small (and commonly seen) changes in pH and

Corresponding author Gary Yellen, gary_yellen@hms.harvard.edu.

temperature, are often overlooked or de-emphasized. A complementary concern is that although an unchanging biosensor signal may indeed indicate that the underlying analyte is unchanging, it can also occur if the biosensor is saturated or de-saturated, due to a poor match between the sensitivity range of the sensor and the physiological range of the target.

Accurate interpretation of a signal therefore requires a clear understanding of both biosensor behavior and the physiological environment in which the biosensor is used. While certain physiological parameters (temperature) can be controlled and monitored, others are more elusive (pH, concentration of ions and other off-target ligands) and require sensor multiplexing. This complicates data collection and analysis and may necessitate the use of sophisticated equipment. It is therefore vital that these scenarios be considered when evaluating which biosensor(s) to use, planning experimental pipelines, and interpreting results. Here, we present common features and caveats of different classes of biosensors, along with experimental considerations and strategies for the responsible use of metabolic biosensors in a physiological context.

Fluorescence intensity imaging

Biosensors convert a change in analyte concentration into a change in fluorescence output. But when comparing the biosensor report from two different cells, it is important to distinguish differences in fluorescence due to analyte concentration from differences in fluorescence due to different levels of biosensor protein expression. The most common way to do this is by “ratiometric” imaging—using the fluorescence measured at two different emission or excitation wavelengths to factor out differences in sensor expression levels. Below, we discuss the slightly different applications of emission ratio or excitation ratio measurements.

A caveat for the use of all ratiometric measurements is that the ratio values measured are often microscope-dependent, due to differences in bandpass filters and in the spectral content of microscope light sources. Comparing measurements between different microscopes requires accurate calibration of the sensor response in each microscope.

Table 1 lists different classes of biosensors that have been used to study metabolism in neurons, arranged by the analyte that they sense; these are also mentioned in context in later sections of this review.

Emission-ratiometric biosensors

Emission-ratiometric biosensors give signals that are measured as the ratio of two different emission wavelengths, generally emitted from two different fluorescent protein (FP) domains in the biosensor. In a “FRET design” biosensor, both FPs are coupled to the sensing or ligand-binding domain, and Förster resonance energy transfer from a “donor” to an “acceptor” FP leads to changes in the emission ratio [4]. Other biosensors use just a single FP coupled to the sensor domain, but a second FP in the same polypeptide provides an unchanging fluorescence signal that allows normalization to compensate for cell-to-cell variation in expression level [5].

Regardless of the particular design, the use of two FPs gives rise to complications that can affect normalization accuracy. For instance, as one images more deeply in a tissue, wavelength-dependent scattering will attenuate shorter wavelengths more than longer wavelengths [6]. This effect can be substantial: an additional 100 μm depth is predicted to give ~10% change in 525 nm : 625 nm emission ratio [7]. Also, commonly observed differences in FP maturation rate or photobleaching can produce different values of the emission ratio in different preparations, or over time in the same preparation.

For FRET sensors, other well-described corrections [4,8,9] are needed to compensate for overlap in excitation and emission spectra of the component FPs, and these corrections are microscope-dependent.

Excitation-ratiometric biosensors

Other sensors exploit the change in excitation spectrum of a single FP that has been coupled to a sensing process; this allows comparison of fluorescence at two different excitation wavelengths to normalize for changes in biosensor concentration. Many sensors in this category use a “circularly permuted” FP (cpFP), in which the original N- and C-termini are joined together and new N- and C-termini are generated near the chromophore. This arrangement permits conformational changes in a scaffold (binding protein) linked to these new N- and C-termini to affect fluorescence by altering the environment surrounding the chromophore.

The use of one FP instead of two resolves many of the issues suffered by two-color FP sensors, and it allows biosensor multiplexing [10–12]. However, the two excitation wavelengths are subject to the same depth-dependent light scattering described in the previous section. For two-photon excitation, for example, an additional 100 μm depth is predicted to decrease the 800 nm : 900 nm ratio by ~20% [7,13].

Unfortunately, the same property that enables excitation-ratio sensing also usually confers a strong pH sensitivity to many cpFP sensors. The WT GFP chromophore exhibits two distinct absorption bands at ~395 nm and ~475 nm, which usually arise from protonated and unprotonated (anionic) species that can be interconverted by pH changes in the physiologic range [14–16]. Activation of the sensor shifts the pKa of the FP and thus the mixture of species, leading to a substantial change in excitation spectrum [3,17–19]. But this same change in excitation spectrum can be mimicked by a simple change in pH, with no change in the sensor target—so that a pure change in pH can masquerade as a change in analyte concentration.

Errors resulting from this pH sensitivity can best be corrected using direct pH measurement by a co-expressed pH sensor [20,21]. A less effective method to control for changes in environment is to do parallel experiments with a “dead” or disabled sensor protein, which will then respond only to changes in pH (hopefully absent!). However, the “dead” sensor tracks the pH sensitivity of only one conformation of the sensor, typically the unliganded form, so that the correction can be incorrect at most analyte concentrations [17,19,22–25].

Environmental changes masquerading as biosensor changes: the problem of aliasing

The pH sensitivity of many cpFP-based biosensors is a specific example of a general problem in which biosensors may report a change in analyte when there has been none: instead, an environmental change alters fluorescence under the “alias” of the analyte. The two most common environmental sensitivities are to pH and temperature changes, although changes in ion concentration can also modify sensor responses. Obviously it is crucial to be aware of such aliasing, and either to control for it or to make an improved biosensor that is more immune to it.

New approaches to sensor design have managed to engineer pH insensitive sensors by using FPs or cpFPs with a low pKa [26–28], but pH sensitivity remains a challenge for many existing sensors. Specific examples of this are provided in later sections of this review.

“Temperature aliasing” is also a concern, as all fluorophores display some degree of temperature sensitivity [29,30] and temperatures in live-cell imaging experiments can change when solutions are exchanged. Fortunately, samples can be temperature controlled, and temperature fluctuations in the bath can be easily monitored during the course of an experiment [31,32]. Subcellular temperature changes, for example inside mitochondria, have been tracked with synthetic probes [33,34].

Table 2 provides details of several typical examples of the pH and temperature aliasing problems based on the literature; these are also mentioned in context below. To help sensor users avoid misinterpretation of their data, it would be ideal for sensor makers to provide information like this—the change in apparent analyte concentration in the physiological range that is produced by a 0.1 unit pH change or a 1°C temperature change—in a readily accessible form.

Fluorescence lifetime imaging

Fluorescence lifetime imaging (FLIM) provides an alternative to ratio imaging that also corrects for variation in biosensor concentration. Fluorescence lifetime is the time between photon absorption and photon emission, *i.e.* the amount of time a fluorophore spends in the excited state. If analyte binding to a biosensor changes the decay rate at which the excited state of the fluorophore returns to the ground state—for instance, by a change in quenching or a change in energy transfer (FRET)—this will be measurable as a change in fluorescence lifetime. Because fluorescence lifetime is independent of fluorescence intensity, there is no need to normalize for expression levels. FLIM uses a single excitation and single emission wavelength, and thus is immune to the wavelength-dependent scattering issues encountered during ratiometric imaging [6,35].

Not all biosensors exhibit a change in fluorescence lifetime. If the biosensor response to analyte binding involves mainly a change in absorbance, or if the unbound state of the sensor is nearly completely non-fluorescent (as in the case of the highly developed GCaMP sensors), no change in lifetime will be measurable. Sometimes biosensors in this category

can be converted to lifetime-readout sensors by swapping out the fluorescent protein or by changing the protein linkers that connect the FP and binding scaffold domains [26,27,35,36].

FRET sensors that exhibit a lifetime change [37,38] can be re-engineered to use less of the visible spectrum by substituting a dim or “dark” acceptor for the longer-wavelength FP that acts as the acceptor [39–44]. This frees up the wavelengths of the emission of the original acceptor for use with a separate biosensor, for multiplexed sensor measurements [9,37].

FLIM sensors, like other sensors, are still subject to aliasing by environmental changes. Higher temperatures typically lead to shorter fluorescence lifetimes. While it is straightforward to control and monitor temperature fluctuations in the bath solution during an experiment, it is much more challenging to calibrate for subcellular temperature changes or pH changes. To address this, a number of FLIM sensors are designed to be resistant to pH [26,27,37]; alternatively, pH and temperature sensors can be used to monitor these changes [33–35].

Fluorescent sensors of metabolism in neurons

We now turn to survey the available biosensors for metabolic parameters in neurons.

Energy demand and production

The metabolic hallmark of neuronal activity is an increased energy demand in response to neurotransmission and the generation of action potentials [45]. To monitor energy consumption and production in response to neuronal activity, a number of sensors have been engineered to track changes in ATP and cellular energy (see Figure 1 and Table 1). The Perceval and PercevalHR [20,46] sensors measure the ratio of ATP to ADP concentration (ATP:ADP), which is directly related to cellular energy charge. The ATeam [38], QUEEN [25] and iATPSnFR [19] families of sensors measure the concentration of ATP itself.

PercevalHR is an excitation-ratiometric sensor constructed by combining a cpVenus with an ATP-binding bacterial regulatory protein, GlnK1 [20,46]. While GlnK1 can bind both ATP and ADP, only ATP binding triggers a substantial conformational change, which is communicated to the cpFP. The high binding affinity for both ATP and ADP ensures that the binding site is always occupied, while the ratio of ATP and ADP concentrations determines which nucleotide is occupying the site, and thus the level of fluorescence output. This is an important measurement in its own right, as ATP:ADP is the driving force for many reactions, can control the direction of flux through metabolic enzymes like phosphoglycerate kinase, and can serve as an indicator of energy production/consumption [20,46].

The ATeam series, on the other hand, is specific for ATP concentration. It utilizes the epsilon subunit of the bacterial F_0F_1-ATP synthase as a scaffold, sandwiching it between two fluorophores to generate an ATP-dependent change in FRET efficiency [38]. QUEEN and iATPSnFR use the same scaffold domain as the ATeams; but instead of a two-fluorophore FRET system, they employ a single circularly permuted fluorescent protein, cpEGFP or cpSFGFP (Superfolder GFP), respectively, to generate changes in fluorescence intensity in response to different ATP concentrations [19,25].

While these fluorescent sensors are quite sensitive and specific, the activity of ATP-dependent enzymes (e.g. kinases and phosphatases) presents a number of experimental challenges in living cells. For example, ATP buffering by creatine kinase (CK) and adenylate kinase (AK) partially masks perturbations in ATP levels in response to external stimuli [47], and the combined action of kinases and phosphatases must be pharmacologically inhibited to achieve accurate sensor calibration in cells [48].

Nevertheless, these sensors have been successfully used to address questions of metabolic responses in neurons. PercevalHR has been used in primary neuronal culture to detect decreases in ATP:ADP in response to metabolic inhibition [20], but showed little response to electrical stimulation simulating short theta bursts [49]. Low affinity variants of ATeam, AT1.03 and AT1.03^{YEMK}, have been used to study the relationship between energy consumption and activity-induced changes in ionic flux [48–51]. High frequency electrical stimulation in the optic nerve [50] and the somatosensory cortex of anesthetized mice [49] generated decreases in the ATP pool that could be captured by AT1.03^{YEMK}.

Beyond the physiological challenges of using ATP sensors, pH and temperature aliasing can be a concern, as discussed above. It has been demonstrated that intracellular pH in neurons acidifies following excitation, up to 0.1–0.2 pH units in response to strong stimulation [52,53]. For PercevalHR, a 0.1 pH increase at a fixed ligand concentration generates a 23% change in sensor output (Table 2) [20], a significant change that could masquerade as a biologically relevant change in ATP:ADP. Co-expression of the red pH sensor pHRed allows for pH bias correction, but requires more sophisticated imaging techniques and precludes multiplexing PercevalHR with other red sensors.

ATeam is largely insensitive to pH changes (less than a 2% increase for a +0.1 pH change, Table 2), but exhibits strong temperature aliasing. AT1.03 experiences a −16% change in output following a 1°C increase in temperature (Table 2). This is largely due to the thermal sensitivity of the small epsilon subunit of the F_0F_1-ATP synthase, but as mentioned above, temperature changes also alter the output of the fluorophore directly.

NADH-NAD$^+$ redox state

Many electron transfer reactions in cells rely on oxidation-reduction of the common cellular cofactor NAD$^+$ and its reduced form, NADH. NADH-NAD$^+$ redox is intrinsically tied to energy status, as it participates both in glycolysis and in oxidative phosphorylation. The cytosolic NADH:NAD$^+$ ratio can inform on the glycolytic state of the cell, conversion of lactate to pyruvate, and mitochondrial shuttling of NADH. Existing NADH sensors are constructed from a single cpFP and the bacterial transcriptional repressor, Rex, taken either from *Thermus aquaticus* (T-Rex) in the case of the NADH:NAD$^+$ sensors Peredox [26] and SoNar [54], or from *Bacillus subtilis* (B-Rex) in the case of the NADH-specific sensor Frex [55]. Rex exists as a homodimer, and each monomer contains its own nucleotide binding pocket. Ligand binding results in transition from an open to a closed conformation.

Both SoNar and Frex utilize cpYFP (pKa ~7.5–8), which imparts the sensors with a strong pH dependence. This can be partially corrected for by normalizing to cpYFP alone [54,55], but as discussed above, this approach does not account for pH-dependent changes of the

liganded form of the sensors and is limited to comparisons of populations of cells. To avoid this problem, Peredox was engineered with a circularly permuted T-Sapphire (pKa ~ 5.6), making it relatively insensitive to pH (−2% change in sensor output for a 0.1 pH increase, Table 2) [26,56]. However, Peredox is sensitive to temperature. Both lifetime and intensity measurements show a 14% signal decrease for every 1ºC increase in temperature (Table 2). Therefore, experimental temperature must be carefully calibrated and controlled to ensure proper quantitation of the Peredox signal. With this in mind, Peredox has been used in slice and *in vivo* to monitor hippocampal NADH:NAD^+, revealing that cytosolic NADH:NAD^+ transiently increases in response to stimulation, reflecting an activity-dependent increase in glucose consumption as opposed to lactate uptake [52].

Fuel preference

Fluorescent biosensors have also been used to explore the fuel preference of neurons and metabolic crosstalk between neurons and glial cells [57–59]. Glucose and lactate (and by extension pyruvate) have been at the core of the discussion on fuel preference in the nervous system [60,61].

Existing glucose sensors are based on bacterial glucose-galactose binding proteins (GGBPs), periplasmic binding proteins that have two lobes connected by a flexible hinge region. Glucose binding occurs at the hinge, bringing the two lobes closer together as the hinge closes around the ligand. The FLIPglu series of glucose sensors takes advantage of the reduction in distance between the two lobes by fusing the *E. coli* GGBP MglB to a CFP/YFP FRET pair [62–65]. The newer Green Glifons (intensity readout) [66] have flanked MglB with a split Citrine to generate a single FP version of that glucose sensor. Similarly, iGlucoSnFR (excitation ratiometric) [67] and iGlucoSnFR-TS (lifetime readout) [27] have single cpFPs inserted into the hinge region of the GGBP of *T. thermophilus* to generate glucose-dependent changes in fluorescence.

Lactate and pyruvate sensors have been constructed from bacterial transcriptional regulators. Like Rex, these regulators are homodimers wherein each monomer contains a ligand binding/regulatory domain and a DNA binding domain. Laconic, a lactate sensor, fuses the *E. coli* lactate-binding domain LldR to the mTFP/Venus FRET pair [68], while Pyronic, a pyruvate sensor, applies a similar strategy to the *E. coli* pyruvate-binding domain PdhR [69].

These sensors have been used in combination to probe fuel consumption in neurons [27,49,52,62,70]. The glucose sensor $FLII^{12}Pglu700\mu\Delta6$ [62] and Laconic showed that neurons co-cultured with astrocytes are fueled both by glucose and lactate [49]. In Drosophila motor neurons, the same sensors along with Pyronic revealed picrotoxin-induced increases in pyruvate and lactate, accompanied by a reduction in intracellular glucose [70]. And in resting neurons in the hippocampus, iGlucoSnFR-TS showed that reducing consumption by partial inhibition of GAPDH elevates the intracellular glucose concentration [27].

Of course, many of these measurements report only on the change in ligand concentration; using fluorescent sensors to measure metabolic fluxes remains a challenge. Changes in flux magnitude can be inferred by pharmacologically separating consumption/production rates

from transport rates [49,52,71]. For example, blocking the glucose transporter GLUT allows the rate of decrease in glucose concentration to be interpreted as the rate of glucose consumption [72,73].

Future Directions

Many exciting sensors for tracking neuronal excitability and cellular metabolism have been developed, but some of the most promising have yet to be used in neurons or intact tissue. These include semisynthetic sensors, like the NAD- and NADP-Snifits, which pair a genetically encoded scaffold with synthetic dyes via a self-labeling SNAP- or HALO-tag to achieve high contrast sensors with improved kinetics [74–76]. Many popular synthetic dyes, like Cy5, are pH insensitive [77], and impressive strides have been made in engineering membrane-permeable dyes that can be used with self-labeling tags [75,78–80]. Other purely synthetic sensors, like the JC-1 indicator of mitochondrial transmembrane potential ($\Delta\psi m$) [81–85], have been valuable tools in studying metabolism in cultured neurons and in slice. Unfortunately, delivery of many dyes into cultured cells or tissues can be difficult, and not all dyes are compatible with the two-photon imaging necessary for imaging in thick, light-scattering brain tissue.

A major advantage of genetically encoded sensors is the ability to control their cellular localization via targeting sequences. Several sensors have been targeted to organelles like the nucleus or the mitochondrion, as well as to different locations within a neuron like axons and dendrites, allowing the study of metabolic compartmentalization within the cell [24,26,35,38,55,86–89]. However, not all sensors are amenable to mitochondrial targeting or membrane immobilization and will require more substantial re-engineering to achieve this kind of manipulation without spoiling the desired sensor properties.

Other genetically encoded sensors for tracking important metabolites like $NADP^+$ or NADPH [24], phosphate [90], citrate [91], α-ketoglutarate [92] and molecular oxygen [93,94] have been made, but have yet to be used in the brain. While this may simply take time, there can also be other reasons including low sensitivity, insufficient signal intensity, or a poor match of the sensor's affinity range to the physiological concentration of metabolites in neurons.

Finally, optimization of new and existing biosensors for robustness against aliasing would be a big leap forward in providing sensors whose responses can be reliably interpreted by all experimenters (and all sensor makers should characterize and communicate clearly the environmental influences on their sensors). Elimination of off-target sensitivities would produce sensors that could be deployed after minimal calibration, either alone or multiplexed, to quantitatively measure critical changes in metabolism and excitability in the brain.

Acknowledgements

This work was supported by grants R01 NS102586 and R01 GM124038 (to G.Y.); F32 NS100331 (to C.M.D.G.) from the NIH/NINDS; and F32 GM123577 (to D.K.) from the NIH/NIGMS.

References and recommended reading

Papers of particular interest, published within the period of review, have been highlighted as:

• of special interest

•• of outstanding interest

1. Abdelfattah AS, Kawashima T, Singh A, Novak O, Liu H, Shuai Y, Huang Y-C, Campagnola L, Seeman SC, Yu J, et al.: Bright and photostable chemigenetic indicators for extended in vivo voltage imaging. Science 2019, 365:699–704. [PubMed: 31371562]
2. Piatkevich KD, Jung EE, Straub C, Linghu C, Park D, Suk H-J, Hochbaum DR, Goodwin D, Pnevmatikakis E, Pak N, et al.: A robotic multidimensional directed evolution approach applied to fluorescent voltage reporters. Nat Chem Biol 2018, 14:352–360. [PubMed: 29483642]
3. Dana H, Sun Y, Mohar B, Hulse BK, Kerlin AM, Hasseman JP, Tsegaye G, Tsang A, Wong A, Patel R, et al.: High-performance calcium sensors for imaging activity in neuronal populations and microcompartments. Nat Methods 2019, 16:649–657. [PubMed: 31209382]
4. Trigo-Mourino P, Thestrup T, Griesbeck O, Griesinger C, Becker S: Dynamic tuning of FRET in a green fluorescent protein biosensor. Sci Adv 2019, 5:eaaw4988. [PubMed: 31457088]
5. Cho J-H, Swanson CJ, Chen J, Li A, Lippert LG, Boye SE, Rose K, Sivaramakrishnan S, Chuong C-M, Chow RH: The GCaMP-R Family of Genetically Encoded Ratiometric Calcium Indicators. ACS Chem Biol 2017, 12:1066–1074. [PubMed: 28195691]
6. Ma L, Jongbloets BC, Xiong W-H, Melander JB, Qin M, Lameyer TJ, Harrison MF, Zemelman BV, Mao T, Zhong H: A Highly Sensitive A-Kinase Activity Reporter for Imaging Neuromodulatory Events in Awake Mice. Neuron 2018, 99:665–679.e5. [PubMed: 30100256]
7. Yellen G, Mongeon R: Quantitative two-photon imaging of fluorescent biosensors. Curr Opin Chem Biol 2015, 27:24–30. [PubMed: 26079046]
8. Ai H, Hazelwood KL, Davidson MW, Campbell RE: Fluorescent protein FRET pairs for ratiometric imaging of dual biosensors. Nat Methods 2008, 5:401–403. [PubMed: 18425137]
9. Demeautis C, Sipieter F, Roul J, Chapuis C, Padilla-Parra S, Riquet FB, Tramier M: Multiplexing PKA and ERK1&2 kinases FRET biosensors in living cells using single excitation wavelength dual colour FLIM. Sci Rep 2017, 7:41026. [PubMed: 28106114]
10. Hertel F, Li S, Chen M, Pott L, Mehta S, Zhang J: Fluorescent Biosensors for Multiplexed Imaging of Phosphoinositide Dynamics. ACS Chem Biol 2020, 15:33–38. [PubMed: 31855412]
11. Mehta S, Zhang Y, Roth RH, Zhang J-F, Mo A, Tenner B, Huganir RL, Zhang J: Single-fluorophore biosensors for sensitive and multiplexed detection of signalling activities. Nat Cell Biol 2018, 20:1215–1225. [PubMed: 30250062]
12. Shcherbakova DM, Stepanenko OV, Turoverov KK, Verkhusha VV: Near-Infrared Fluorescent Proteins: Multiplexing and Optogenetics across Scales. Trends Biotechnol 2018, 36:1230–1243. [PubMed: 30041828]
13. Horton NG, Wang K, Kobat D, Clark CG, Wise FW, Schaffer CB, Xu C: In vivo three-photon microscopy of subcortical structures within an intact mouse brain. Nat Photonics 2013, 7.
14. Heim R, Prasher DC, Tsien RY: Wavelength mutations and posttranslational autoxidation of green fluorescent protein. Proc Natl Acad Sci USA 1994, 91:12501–12504. [PubMed: 7809066]
15. Cubitt AB, Heim R, Adams SR, Boyd AE, Gross LA, Tsien RY: Understanding, improving and using green fluorescent proteins. Trends Biochem Sci 1995, 20:448–455. [PubMed: 8578587]
16. Tsien RY: The green fluorescent protein. Annu Rev Biochem 1998, 67:509–544. [PubMed: 9759496]
17. Borden PM, Zhang P, Shivange AV, Marvin JS, Cichon J, Dan C, Podgorski K, Figueiredo A, Novak O, Tanimoto M, et al.: A fast genetically encoded fluorescent sensor for faithful in vivo acetylcholine detection in mice, fish, worms and flies. bioRxiv 2020, doi:10.1101/2020.02.07.939504.

18. Barnett LM, Hughes TE, Drobizhev M: Deciphering the molecular mechanism responsible for GCaMP6m's Ca2+-dependent change in fluorescence. PLoS ONE 2017, 12:e0170934. [PubMed: 28182677]
19. Lobas MA, Tao R, Nagai J, Kronschläger MT, Borden PM, Marvin JS, Looger LL, Khakh BS: A genetically encoded single-wavelength sensor for imaging cytosolic and cell surface ATP. Nat Commun 2019, 10:711. [PubMed: 30755613]
20. Tantama M, Martínez-François JR, Mongeon R, Yellen G: Imaging energy status in live cells with a fluorescent biosensor of the intracellular ATP-to-ADP ratio. Nat Commun 2013, 4:2550. [PubMed: 24096541]
21. Rajendran M, Claywell B, Haynes EP, Scales U, Henning CK, Tantama M: Imaging pH Dynamics Simultaneously in Two Cellular Compartments Using a Ratiometric pH-Sensitive Mutant of mCherry. ACS Omega 2018, 3:9476–9486. [PubMed: 30197999]
22. Mendelsohn BA, Bennett NK, Darch MA, Yu K, Nguyen MK, Pucciarelli D, Nelson M, Horlbeck MA, Gilbert LA, Hyun W, et al.: A high-throughput screen of real-time ATP levels in individual cells reveals mechanisms of energy failure. PLoS Biol 2018, 16:e2004624. [PubMed: 30148842]
23. Cameron WD, Bui CV, Hutchinson A, Loppnau P, Gräslund S, Rocheleau JV: Apollo-NADP(+): a spectrally tunable family of genetically encoded sensors for NADP(+). Nat Methods 2016, 13:352–358. [PubMed: 26878383]
24. Tao R, Zhao Y, Chu H, Wang A, Zhu J, Chen X, Zou Y, Shi M, Liu R, Su N, et al.: Genetically encoded fluorescent sensors reveal dynamic regulation of NADPH metabolism. Nat Methods 2017, 14:720–728. [PubMed: 28581494]
25. Yaginuma H, Kawai S, Tabata KV, Tomiyama K, Kakizuka A, Komatsuzaki T, Noji H, Imamura H: Diversity in ATP concentrations in a single bacterial cell population revealed by quantitative single-cell imaging. Sci Rep 2014, 4:6522. [PubMed: 25283467]
26. Hung YP, Albeck JG, Tantama M, Yellen G: Imaging cytosolic NADH-NAD(+) redox state with a genetically encoded fluorescent biosensor. Cell Metab 2011, 14:545–554. [PubMed: 21982714]
27. Díaz-García CM, Lahmann C, Martínez-François JR, Li B, Koveal D, Nathwani N, Rahman M, Keller JP, Marvin JS, Looger LL, et al.: Quantitative in vivo imaging of neuronal glucose concentrations with a genetically encoded fluorescence lifetime sensor. J Neurosci Res 2019, 97:946–960. [PubMed: 31106909]
28. Botman D, de Groot DH, Schmidt P, Goedhart J, Teusink B: In vivo characterisation of fluorescent proteins in budding yeast. Sci Rep 2019, 9:2234. [PubMed: 30783202]
29. McAnaney TB, Shi X, Abbyad P, Jung H, Remington SJ, Boxer SG: Green fluorescent protein variants as ratiometric dual emission pH sensors. 3. Temperature dependence of proton transfer. Biochemistry 2005, 44:8701–8711. [PubMed: 15952777]
30. Chi W, Yin W, Qi Q, Qiao Q, Lin Y, Zhu Z, Vijayan S, Hashimoto M, Udayakumar G, Xu Z, et al.: Ground-state conformers enable bright single-fluorophore ratiometric thermometers with positive temperature coefficients. Materials Chemistry Frontiers 2017, 1:2383–2390.
31. Nakano M, Arai Y, Kotera I, Okabe K, Kamei Y, Nagai T: Genetically encoded ratiometric fluorescent thermometer with wide range and rapid response. PLoS ONE 2017, 12:e0172344. [PubMed: 28212432]
32. Maksimov EG, Yaroshevich IA, Tsoraev GV, Sluchanko NN, Slutskaya EA, Shamborant OG, Bobik TV, Friedrich T, Stepanov AV: A genetically encoded fluorescent temperature sensor derived from the photoactive Orange Carotenoid Protein. Sci Rep 2019, 9:8937. [PubMed: 31222180]
33. Qiao J, Chen C, Shangguan D, Mu X, Wang S, Jiang L, Qi L: Simultaneous Monitoring of Mitochondrial Temperature and ATP Fluctuation Using Fluorescent Probes in Living Cells. Anal Chem 2018, 90:12553–12558. [PubMed: 30295464]
34. Chrétien D, Bénit P, Ha H-H, Keipert S, El-Khoury R, Chang Y-T, Jastroch M, Jacobs HT, Rustin P, Rak M: Mitochondria are physiologically maintained at close to 50 °C. PLoS Biol 2018, 16:e2003992. [PubMed: 29370167]
35. Tantama M, Hung YP, Yellen G: Imaging intracellular pH in live cells with a genetically encoded red fluorescent protein sensor. J Am Chem Soc 2011, 133:10034–10037. [PubMed: 21631110]

36. Mongeon R, Venkatachalam V, Yellen G: Cytosolic NADH-NAD(+) Redox Visualized in Brain Slices by Two-Photon Fluorescence Lifetime Biosensor Imaging. Antioxid Redox Signal 2016, 25:553–563. [PubMed: 26857245]
37. Chen Y, Saulnier JL, Yellen G, Sabatini BL: A PKA activity sensor for quantitative analysis of endogenous GPCR signaling via 2-photon FRET-FLIM imaging. Front Pharmacol 2014, 5:56. [PubMed: 24765076]
38. Imamura H, Nhat KPH, Togawa H, Saito K, Iino R, Kato-Yamada Y, Nagai T, Noji H: Visualization of ATP levels inside single living cells with fluorescence resonance energy transfer-based genetically encoded indicators. Proc Natl Acad Sci USA 2009, 106:15651–15656. [PubMed: 19720993]
39. Murakoshi H, Shibata ACE, Nakahata Y, Nabekura J: A dark green fluorescent protein as an acceptor for measurement of Förster resonance energy transfer. Sci Rep 2015, 5:15334. [PubMed: 26469148]
40. Murakoshi H, Horiuchi H, Kosugi T, Onda M, Sato A, Koga N, Nabekura J: ShadowR: a novel chromoprotein with reduced non-specific binding and improved expression in living cells. Sci Rep 2019, 9:12072. [PubMed: 31427680]
41. Murakoshi H, Shibata ACE: ShadowY: a dark yellow fluorescent protein for FLIM-based FRET measurement. Sci Rep 2017, 7:6791. [PubMed: 28754922]
42. Ganesan S, Ameer-Beg SM, Ng TTC, Vojnovic B, Wouters FS: A dark yellow fluorescent protein (YFP)-based Resonance Energy-Accepting Chromoprotein (REACh) for Förster resonance energy transfer with GFP. Proc Natl Acad Sci USA 2006, 103:4089–4094. [PubMed: 16537489]
43. Murakoshi H, Lee S-J, Yasuda R: Highly sensitive and quantitative FRET-FLIM imaging in single dendritic spines using improved non-radiative YFP. Brain Cell Biol 2008, 36:31–42. [PubMed: 18512154]
44. Pettikiriarachchi A, Gong L, Perugini MA, Devenish RJ, Prescott M: Ultramarine, a chromoprotein acceptor for Förster resonance energy transfer. PLoS ONE 2012, 7:e41028. [PubMed: 22815901]
45. Attwell D, Laughlin SB: An energy budget for signaling in the grey matter of the brain. J Cereb Blood Flow Metab 2001, 21:1133–1145. [PubMed: 11598490]
46. Berg J, Hung YP, Yellen G: A genetically encoded fluorescent reporter of ATP:ADP ratio. Nat Methods 2009, 6:161–166. [PubMed: 19122669]
47. Erecińska M, Silver IA: ATP and brain function. J Cereb Blood Flow Metab 1989, 9:2–19. [PubMed: 2642915]
48. Gerkau NJ, Lerchundi R, Nelson JSE, Lantermann M, Meyer J, Hirrlinger J, Rose CR: Relation between activity-induced intracellular sodium transients and ATP dynamics in mouse hippocampal neurons. J Physiol (Lond) 2019, 597:5687–5705. [PubMed: 31549401] • Gerkau et al. use ATeam1.03YEMK to characterize transient ATP decreases in the somata and dendrites of CA1 neurons from acute hippocampal slices. Using a Na+-sensitive fluorescent dye, the authors also explore how Na+ fluxes impact energy demand upon stimulation. A calibration of ATeam1.03YEMK performed in permeabilized neurons highlights some of the obstacles faced when attempting absolute quantification of analytes based on biosensor readouts, as the in-cell calibration yields a lower apparent affinity and temperature sensitivity relative to the in vitro calibration.
49. Baeza-Lehnert F, Saab AS, Gutiérrez R, Larenas V, Díaz E, Horn M, Vargas M, Hösli L, Stobart J, Hirrlinger J, et al.: Non-Canonical Control of Neuronal Energy Status by the Na+ Pump. Cell Metab 2019, 29:668–680.e4. [PubMed: 30527744]
50. Trevisiol A, Saab AS, Winkler U, Marx G, Imamura H, Möbius W, Kusch K, Nave K-A, Hirrlinger J: Monitoring ATP dynamics in electrically active white matter tracts. Elife 2017, 6.•• This paper is the first to present a transgenic mouse stably expressing a genetically encoded metabolic biosensor. ATeam1.03YEMK is expressed pan-neuronally, allowing Trevisiol et al to detect dips in the ATP pool in response to sustained, high frequency electrical stimulation in the optic nerve. The authors also probe the role of different fuels (glucose, lactate and pyruvate) in electrical activity and ATP homeostasis, concluding that lactate movement across monocarboxylate transporters is required for ATP homeostasis in active myelinated fibers.

51. Lerchundi R, Kafitz KW, Winkler U, Färfers M, Hirrlinger J, Rose CR: FRET-based imaging of intracellular ATP in organotypic brain slices. J Neurosci Res 2019, 97:933–945. [PubMed: 30506574]
52. Díaz-García CM, Mongeon R, Lahmann C, Koveal D, Zucker H, Yellen G: Neuronal Stimulation Triggers Neuronal Glycolysis and Not Lactate Uptake. Cell Metab 2017, 26:361–374.e4. [PubMed: 28768175] •• This paper describes transient increases in the cytosolic NADH:NAD+ ratio in stimulated neurons in acute brain slices and in vivo using the fluorescence lifetime sensor Peredox paired with the calcium sensor RCaMP1h (here, used as a lifetime-readout sensor instead of an intensity-readout sensor). This, along with a readout of lactate concentrations from the FRET sensor Laconic, provide evidence in favor of direct neuronal glycolysis, as opposed to neuronal import of lactate from astrocytes.
53. Raimondo JV, Tomes H, Irkle A, Kay L, Kellaway L, Markram H, Millar RP, Akerman CJ: Tight Coupling of Astrocyte pH Dynamics to Epileptiform Activity Revealed by Genetically Encoded pH Sensors. J Neurosci 2016, 36:7002–7013. [PubMed: 27358457]
54. Zhao Y, Hu Q, Cheng F, Su N, Wang A, Zou Y, Hu H, Chen X, Zhou H-M, Huang X, et al.: SoNar, a Highly Responsive NAD+/NADH Sensor, Allows High-Throughput Metabolic Screening of Anti-tumor Agents. Cell Metab 2015, 21:777–789. [PubMed: 25955212]
55. Zhao Y, Jin J, Hu Q, Zhou H-M, Yi J, Yu Z, Xu L, Wang X, Yang Y, Loscalzo J: Genetically encoded fluorescent sensors for intracellular NADH detection. Cell Metab 2011, 14:555–566. [PubMed: 21982715]
56. Zapata-Hommer O, Griesbeck O: Efficiently folding and circularly permuted variants of the Sapphire mutant of GFP. BMC Biotechnol 2003, 3:5. [PubMed: 12769828]
57. Yellen G: Fueling thought: Management of glycolysis and oxidative phosphorylation in neuronal metabolism. J Cell Biol 2018, 217:2235–2246. [PubMed: 29752396]
58. Barros LF, Bolaños JP, Bonvento G, Bouzier-Sore A-K, Brown A, Hirrlinger J, Kasparov S, Kirchhoff F, Murphy AN, Pellerin L, et al.: Current technical approaches to brain energy metabolism. Glia 2018, 66:1138–1159. [PubMed: 29110344]
59. Magistretti PJ, Allaman I: Lactate in the brain: from metabolic end-product to signalling molecule. Nat Rev Neurosci 2018, 19:235–249. [PubMed: 29515192]
60. Barros LF, Weber B: CrossTalk proposal: an important astrocyte-to-neuron lactate shuttle couples neuronal activity to glucose utilisation in the brain. J Physiol (Lond) 2018, 596:347–350. [PubMed: 29292516]
61. Bak LK, Walls AB: CrossTalk opposing view: lack of evidence supporting an astrocyte-to-neuron lactate shuttle coupling neuronal activity to glucose utilisation in the brain. J Physiol (Lond) 2018, 596:351–353. [PubMed: 29292507]
62. Takanaga H, Chaudhuri B, Frommer WB: GLUT1 and GLUT9 as major contributors to glucose influx in HepG2 cells identified by a high sensitivity intramolecular FRET glucose sensor. Biochim Biophys Acta 2008, 1778:1091–1099. [PubMed: 18177733]
63. Deuschle K, Chaudhuri B, Okumoto S, Lager I, Lalonde S, Frommer WB: Rapid metabolism of glucose detected with FRET glucose nanosensors in epidermal cells and intact roots of Arabidopsis RNA-silencing mutants. Plant Cell 2006, 18:2314–2325. [PubMed: 16935985]
64. Deuschle K, Okumoto S, Fehr M, Looger LL, Kozhukh L, Frommer WB: Construction and optimization of a family of genetically encoded metabolite sensors by semirational protein engineering. Protein Sci 2005, 14:2304–2314. [PubMed: 16131659]
65. Fehr M, Lalonde S, Lager I, Wolff MW, Frommer WB: In vivo imaging of the dynamics of glucose uptake in the cytosol of COS-7 cells by fluorescent nanosensors. J Biol Chem 2003, 278:19127–19133. [PubMed: 12649277]
66. Mita M, Ito M, Harada K, Sugawara I, Ueda H, Tsuboi T, Kitaguchi T: Green Fluorescent Protein-Based Glucose Indicators Report Glucose Dynamics in Living Cells. Anal Chem 2019, 91:4821–4830. [PubMed: 30869867]
67. Keller JP, Marvin JS, Lacin H, Lemon WC, Shea J, Kim S, Lee RT, Koyama M, Keller PJ, Looger LL: In vivo glucose imaging in multiple model organisms with an engineered single-wavelength sensor. bioRxiv 2019, doi:10.1101/571422.• Keller et al. report a new family of green fluorescent glucose sensors spanning a sensing range of ~0.3 μM to ~100 mM glucose, which can be

multiplexed with red calcium sensors. The authors demonstrate that these sensors can be expressed in several biological preparations from different species. In particular, they study the responsiveness of the sensor in co-cultures of neurons and astrocytes when exposed to oscillating external glucose.

68. San Martín A, Ceballo S, Ruminot I, Lerchundi R, Frommer WB, Barros LF: A genetically encoded FRET lactate sensor and its use to detect the Warburg effect in single cancer cells. PLoS ONE 2013, 8:e57712. [PubMed: 23469056]
69. San Martín A, Ceballo S, Baeza-Lehnert F, Lerchundi R, Valdebenito R, Contreras-Baeza Y, Alegría K, Barros LF: Imaging mitochondrial flux in single cells with a FRET sensor for pyruvate. PLoS ONE 2014, 9:e85780. [PubMed: 24465702]
70. González-Gutiérrez A, Ibacache A, Esparza A, Barros LF, Sierralta J: Neuronal lactate levels depend on glia-derived lactate during high brain activity in Drosophila. Glia 2019, doi:10.1002/glia.23772.
71. Conley JM, Radhakrishnan S, Valentino SA, Tantama M: Imaging extracellular ATP with a genetically-encoded, ratiometric fluorescent sensor. PLoS ONE 2017, 12:e0187481. [PubMed: 29121644]
72. Bittner CX, Loaiza A, Ruminot I, Larenas V, Sotelo-Hitschfeld T, Gutiérrez R, Córdova A, Valdebenito R, Frommer WB, Barros LF: High resolution measurement of the glycolytic rate. Front Neuroenergetics 2010, 2.
73. San Martín A, Sotelo-Hitschfeld T, Lerchundi R, Fernández-Moncada I, Ceballo S, Valdebenito R, Baeza-Lehnert F, Alegría K, Contreras-Baeza Y, Garrido-Gerter P, et al.: Single-cell imaging tools for brain energy metabolism: a review. Neurophotonics 2014, 1:011004. [PubMed: 26157964]
74. Sallin O, Reymond L, Gondrand C, Raith F, Koch B, Johnsson K: Semisynthetic biosensors for mapping cellular concentrations of nicotinamide adenine dinucleotides. Elife 2018, 7.
75. Thirukkumaran OM, Wang C, Asouzu NJ, Fron E, Rocha S, Hofkens J, Lavis LD, Mizuno H: Improved HaloTag Ligand Enables BRET Imaging With NanoLuc. Front Chem 2019, 7:938. [PubMed: 31993413]
76. Deo C, Abdelfattah AS, Bhargava HK, Berro AJ, Falco N, Moeyaert B, Chupanova M, Lavis LD, Schreiter ER: Bright and tunable far-red chemigenetic indicators. bioRxiv 2020, doi:10.1101/2020.01.08.898783.
77. Johnson ID: Practical Considerations in the Selection and Application of Fluorescent Probes In Handbook Of Biological Confocal Microscopy. Edited by Pawley JB. Springer US; 2006:353–367.
78. Grimm JB, English BP, Chen J, Slaughter JP, Zhang Z, Revyakin A, Patel R, Macklin JJ, Normanno D, Singer RH, et al.: A general method to improve fluorophores for live-cell and single-molecule microscopy. Nat Methods 2015, 12:244–250, 3 p following 250. [PubMed: 25599551]
79. Grimm JB, Muthusamy AK, Liang Y, Brown TA, Lemon WC, Patel R, Lu R, Macklin JJ, Keller PJ, Ji N, et al.: A general method to fine-tune fluorophores for live-cell and in vivo imaging. Nat Methods 2017, 14:987–994. [PubMed: 28869757]
80. Grimm JB, Brown TA, English BP, Lionnet T, Lavis LD: Synthesis of Janelia Fluor HaloTag and SNAP-Tag Ligands and Their Use in Cellular Imaging Experiments. Methods Mol Biol 2017, 1663:179–188. [PubMed: 28924668]
81. Reers M, Smith TW, Chen LB: J-aggregate formation of a carbocyanine as a quantitative fluorescent indicator of membrane potential. Biochemistry 1991, 30:4480–4486. [PubMed: 2021638]
82. Smiley ST, Reers M, Mottola-Hartshorn C, Lin M, Chen A, Smith TW, Steele GD, Chen LB: Intracellular heterogeneity in mitochondrial membrane potentials revealed by a J-aggregate-forming lipophilic cation JC-1. Proc Natl Acad Sci USA 1991, 88:3671–3675. [PubMed: 2023917]
83. Rivero-Segura NA, Coronado-Mares MI, Rincón-Heredia R, Pérez-Torres I, Montiel T, Pavón N, Cabrera-Reyes EA, Massieu L, Cerbón M: Prolactin prevents mitochondrial dysfunction induced by glutamate excitotoxicity in hippocampal neurons. Neurosci Lett 2019, 701:58–64. [PubMed: 30790645]

84. Zheng L, Bernard-Marissal N, Moullan N, D'Amico D, Auwerx J, Moore DJ, Knott G, Aebischer P, Schneider BL: Parkin functionally interacts with PGC-1α to preserve mitochondria and protect dopaminergic neurons. Hum Mol Genet 2017, 26:582–598. [PubMed: 28053050]

85. Wang B, Zhang X, Wang C, Chen L, Xiao Y, Pang Y: Bipolar and fixable probe targeting mitochondria to trace local depolarization via two-photon fluorescence lifetime imaging. Analyst 2015, 140:5488–5494. [PubMed: 26160675]

86. Arce-Molina R, Cortés-Molina F, Sandoval PY, Galaz A, Alegría K, Schirmeier S, Barros LF, Martín AS: A highly responsive pyruvate sensor reveals pathway-regulatory role of the mitochondrial pyruvate carrier MPC. bioRxiv 2019, doi:10.1101/611806.• Arce-Molina et al. describe a novel single-fluorophore pyruvate sensor (PyronicSF) with enhanced dynamic and sensing ranges realtive to its FRET-based predecessor Pyronic. The authors effectively targeted this sensor to the mitochondria of glial cells and estimated pyruvate consumption rates upon inhibition of the mitochondrial pyruvate carrier. The authors also provide a method for correcting for the pH-sensitivity of the sensor.

87. Broussard GJ, Liang Y, Fridman M, Unger EK, Meng G, Xiao X, Ji N, Petreanu L, Tian L: In vivo measurement of afferent activity with axon-specific calcium imaging. Nat Neurosci 2018, 21:1272–1280. [PubMed: 30127424]

88. Yoshida T, Alfaqaan S, Sasaoka N, Imamura H: Application of FRET-Based Biosensor "ATeam" for Visualization of ATP Levels in the Mitochondrial Matrix of Living Mammalian Cells. Methods Mol Biol 2017, 1567:231–243. [PubMed: 28276022]

89. Shivange AV, Borden PM, Muthusamy AK, Nichols AL, Bera K, Bao H, Bishara I, Jeon J, Mulcahy MJ, Cohen B, et al.: Determining the pharmacokinetics of nicotinic drugs in the endoplasmic reticulum using biosensors. J Gen Physiol 2019, 151:738–757. [PubMed: 30718376]

90. Gu H, Lalonde S, Okumoto S, Looger LL, Scharff-Poulsen AM, Grossman AR, Kossmann J, Jakobsen I, Frommer WB: A novel analytical method for in vivo phosphate tracking. FEBS Lett 2006, 580:5885–5893. [PubMed: 17034793]

91. Ewald JC, Reich S, Baumann S, Frommer WB, Zamboni N: Engineering genetically encoded nanosensors for real-time in vivo measurements of citrate concentrations. PLoS ONE 2011, 6:e28245. [PubMed: 22164251]

92. Lüddecke J, Francois L, Spät P, Watzer B, Chilczuk T, Poschet G, Hell R, Radlwimmer B, Forchhammer K: PII Protein-Derived FRET Sensors for Quantification and Live-Cell Imaging of 2-Oxoglutarate. Sci Rep 2017, 7:1437. [PubMed: 28469248]

93. Penjweini R, Andreoni A, Rosales T, Kim J, Brenner MD, Sackett DL, Chung JH, Knutson JR: Intracellular oxygen mapping using a myoglobin-mCherry probe with fluorescence lifetime imaging. J Biomed Opt 2018, 23:1–14.

94. Nomata J, Hisabori T: Development of heme protein based oxygen sensing indicators. Sci Rep 2018, 8:11849. [PubMed: 30087408]

95. Mächler P, Wyss MT, Elsayed M, Stobart J, Gutierrez R, von Faber-Castell A, Kaelin V, Zuend M, San Martín A, Romero-Gómez I, et al.: In Vivo Evidence for a Lactate Gradient from Astrocytes to Neurons. Cell Metab 2016, 23:94–102. [PubMed: 26698914]

Highlights

1. Genetically encoded biosensors give quantitative readouts of key brain metabolites
2. Biosensors allow investigation of the relationship between activity and metabolism
3. Environmental changes (pH, temperature) can masquerade as changes in analyte

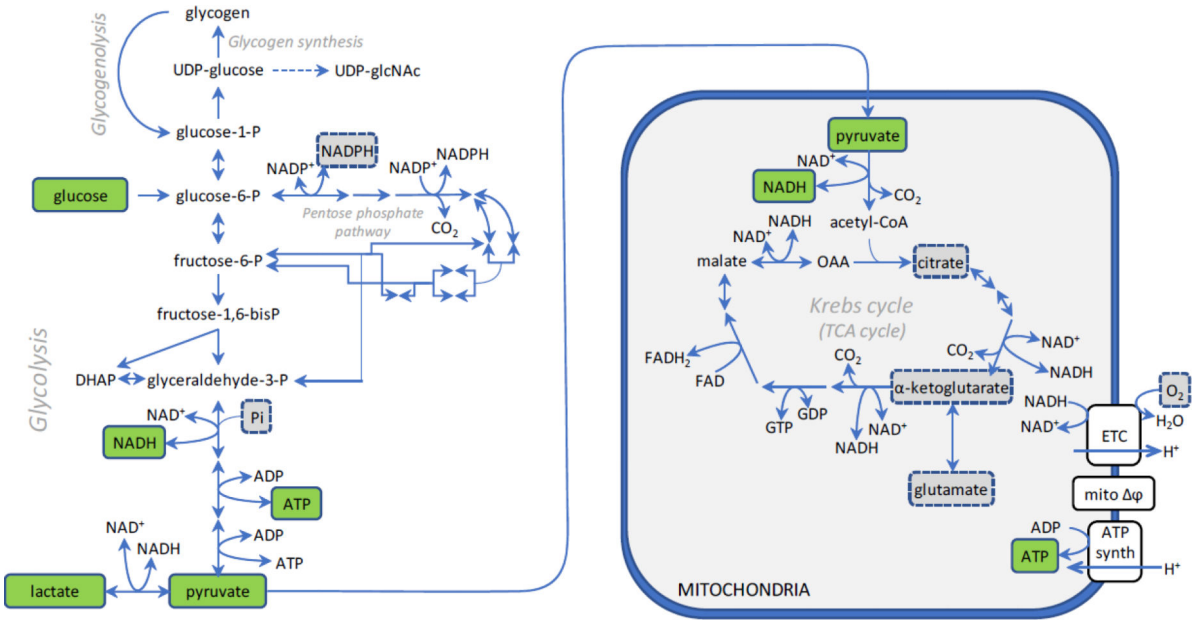

Figure 1. Metabolic targets of fluorescent biosensors in neurons

Key substrates, intermediates and cofactors in brain energy metabolism are presented in this diagram of neuronal metabolism. Solid green boxes indicate analytes that have been successfully measured using genetically encoded fluorescent biosensors expressed in the cytosol and mitochondrial matrix of neurons. Dashed gray boxes indicate target analytes of existing sensors that have not yet been utilized in neurons.

Cytosolic measurements of pyruvate, lactate and glucose have been essential in studying fuel preference in neurons at rest and during stimulation, while NADH:NAD^+ and ATP sensors have provided insight into the relationship between excitability and energy demand. Targeting sensors to intracellular organelles like the mitochondria have enabled study of the compartmentation of energy production. In the future, biosensors for analytes like NADPH, inorganic phosphate, citrate, α-ketoglutarate, mitochondrial glutamate and O_2 could further inform on the cellular energy state and the overall redox state in neurons.

Table 1:

Genetically encoded fluorescent biosensors used for the study of neuronal metabolism

Sensor	Scaffold	Fluorescent Protein(s)	Excitation *a*	Emission *a*	Sensor Design	Dynamic range: fold change or Δ lifetime	Affinity (K_d or K_R)	Reference
ATP								
ATeam1.03	F_0F_1-ATP synthase, ε subunit *(B. subtilis)*	mseCFP/ mVenus	435 nm (D)	475 nm (D) 527 nm (A)	FRET	2.3-fold (37°C)	3.3 mM	[38]
ATeam1.03^{YEMK}	F_0F_1-ATP synthase, ε subunit *(B. subtilis)*	mseCFP/ mVenus	435 nm (D)	475 nm (D) 527 nm (A)	FRET	n.r.	1.2 mM (37°C) 2.6 mM (20–22°C) *b*	[38] [48]
QUEEN-2m	F_0F_1-ATP synthase, ε subunit *(B. subtilis)*	cp-EGFP	400 nm / 494 nm	513 nm	Ratiometric (excitation)	>3-fold (25°C)	2.4 mM	[25]
QUEEN-7μ	F_0F_1-ATP synthase, ε subunit *(B.* PS3*)*	cp-EGFP	400 nm / 494 nm	513 nm	Ratiometric (excitation)	~4.3-fold (37°C) ~5-fold (25°C)	14 μM 7.2 μM	[25]
iATPSnFR$^{1.0}$	F_0F_1-ATP synthase, ε subunit *(B.* PS3*)*	cp-SFGFP	488 nm	515 nm	Intensity	2-fold (RT)	350 μM	[19]
iATPSnFR$^{1.1}$	F_0F_1-ATP synthase, ε subunit *(B.* PS3*)*	cp-SFGFP	488 nm	515 nm	Intensity	1.88-fold (RT)	138 μM	[19]
ATP:ADP								
PercevalHR	GlnK, nucleotide binding protein (*M. jannaschii*)	cp-mVenus	482 nm / 455 nm	529 nm	Ratiometric (excitation)	4.6-fold (37°C) ~4-fold (RT)	ATP:ADP ≈ 6.1 ATP:ADP ≈ 3.5	[20]
NADH								
Frex	B-Rex, NADH binding protein (*B. subtilis*)	cpYFP	488 nm / 405 nm	525 nm	Ratiometric (excitation)	~9.5-fold (RT)	3.7 μM	[55]
NADH:NAD$^+$								
SoNar	T-Rex, NADH binding protein (*T. aquaticus*)	cpYFP	420 nm / 485 nm	528 nm	Ratiometric (excitation)	~15-fold (RT)	NADH:NAD$^+$ ≈ 1/40	[54]
Peredox	T-Rex, NADH binding protein (*T. aquaticus*)	cp-T-Sapphire	400 nm	510 nm	Intensity *b*	2.5-fold (35°C)	NADH:NAD$^+$ ≈ 1/90	[26]
			800 nm (two-photon)	525 nm	Lifetime	0.9 ns (35°C) 0.8 ns (25°C)	NADH:NAD$^+$ ≈ 1/255 NADH:NAD$^+$ ≈ 1/529	[36]
Glucose								
FLII^{12}Pglu700μΔ6	MglB, glucose/ galactose	eCFP/ Citrine	433 nm (D)	485 nm (D)	FRET	1.5-fold (RT)	660 μM	[62]

Sensor	Scaffold	Fluorescent Protein(s)	Excitation *a*	Emission *a*	Sensor Design	Dynamic range: fold change or Δ lifetime	Affinity (K_d or K_R)	Reference
	binding protein (*E. coli*)			528 nm (A)				
Green Glifon600	MglB, glucose/ galactose binding protein (*E. coli*)	Citrine	480 nm	530 nm	Intensity	~5-fold (RT)	590 μM	[66]
Green Glifon4000	MglB, glucose/ galactose binding protein (*E. coli*)	Citrine	480 nm	530 nm	Intensity	~6-fold (RT)	3.8 mM	[66]
iGlucoSnFR	GGBP, glucose/ galactose binding protein (*T. thermophilus*)	cpGFP	485 nm	515 nm	Intensity	3.32-fold (RT)	7.7 mM	[67]
iGlucoSnFR-TS	GGBP, glucose/ galactose binding protein (*T. thermophilus*)	cp-T-Sapphire	790 nm (two-photon)	525 nm	Lifetime	0.34 ns (37°C) 0.38 ns (37°C)[c]	2.2 mM 1.8 mM [c]	[27]
Lactate								
Laconic	LldR, lactate binding transcription regulator (*E. coli*)	mTFP/ Venus	430 nm (D)	480 nm (D) 535 nm (A)	FRET	~1.2-fold (25°C)	Biphasic: K_1 = 8 μM K_2 = 830 μM	[68]
Pyruvate								
Pyronic	PdhR, pyruvate dehydrogenase complex repressor (*E. coli*)	mTFP/ Venus	430 nm (D)	480 nm (D) 535 nm (A)	FRET	~1.24-fold (RT)	107 μM	[69]

D: *FRET donor*; A: *FRET acceptor*; n.r.: *not reported*; RT: *room temperature*

[a] The provided excitation and emission wavelengths refer to the imaging parameters used in the referenced article, which may differ from the peak excitation and emission wavelengths of the solitary fluorophore(s).

[b] Peredox intensity can be normalized for different expression levels in cells by fusing the sensor with an analyte and pH insensitive fluorescent protein (e.g. citrine or mCherry). Then, the readout of the sensor is reported as the emission ratio of the two fluorescent proteins (sensor/reference).

[c] This calibration was performed in permeabilized cells. Unless otherwise stated, all other calibrations in this table were performed *in vitro*.

Table 2:

Aliasing effects of temperature and pH on representative biosensors used for the study of neuronal metabolism

Sensor	Dynamic range: fold change or Δ lifetime	Affinity (K_d or K_R)	ALIASING: Change in apparent [analyte] +0.1 pH	+1°C	References
ATP					
ATeam 1.03	2.3-fold (37°C)	3.3 mM	**+1.7%**	**−16%**	[38]
ATP:ADP					
PercevalHR	4.6-fold (37°C)	ATP:ADP ≈ 6.1	**+23%**	**−3.6%**	[20]
NADH:NAD$^+$					
Peredox	2.5-fold (35°C)	NADH:NAD$^+$ ≈ 1/90	**−2.0%**	**−15%**	[26]
	0.9 ns (35°C)	NADH:NAD$^+$ ≈ 1/255	**−1.6%**	**−14%**	[36]
Lactate					
Laconic	~1.2-fold (25°C)	Biphasic: K_1 = 8 μM K_2 = 830 μM [a]	**−48%**	**−8.3%**	[68] [95][b]

Approximate aliasing effects were estimated at the $K_{0.5}$ of each sensor, as calculated for near-physiologic pH (7.2–7.4) and the temperatures specified between parenthesis in the field for the dynamic range. Because of non-linear effects on the sensor readout, percentage changes for stronger perturbations (higher than 1°C or 0.1 pH units), or at different [analyte], may deviate from the values reported here.

[a] For simplicity, the dose-response curves for Laconic were fitted to a Hill equation and the aliasing effects of temperature and pH were estimated at [lactate] = 1 mM. The fitted curves presented Hill coefficients < 1, suggesting that Laconic have two binding sites with negative cooperativity.

[b] This study was only used to estimate the effect of temperature.